

Applications of DFT+DMFT in Materials Science

Arpita Paul,¹ Turan Birol^{1,*}

¹Department of Chemical Engineering and Materials Science, University of Minnesota, Minneapolis, Minnesota 55455, USA

*e-mail: tbirol@umn.edu

Xxxx. Xxx. Xxx. Xxx. Yyyy. Aa:1–24

[https://doi.org/10.1146/\(\(please add article doi\)\)](https://doi.org/10.1146/((please add article doi)))

Copyright © Yyyy by Annual Reviews.
All rights reserved

Keywords

first principles calculations, density functional theory, dynamical mean field theory, correlated materials

Abstract

First principles methods can provide insight into materials that otherwise is impossible to acquire. Density Functional Theory (DFT) has been the first principles method of choice for numerous applications, but it falls short of predicting the properties of correlated materials. First principles Density Functional Theory + Dynamical Mean Field Theory (DFT+DMFT) is a powerful tool that can address these shortcomings of DFT when applied to correlated metals. In this brief review, which is aimed at non-experts, we review the basics and some applications of DFT+DMFT.

Contents

1. INTRODUCTION	2
2. DFT, DMFT, and DFT+DMFT	3
2.1. Density Functional Theory	3
2.2. Dynamical Mean Field Theory	5
2.3. First Principles DFT+DMFT	7
3. MASS RENORMALIZATION IN CORRELATED METALS	9
4. CRYSTAL STRUCTURES AND LATTICE RESPONSE FROM DFT+DMFT	12
4.1. Error in lattice parameters of correlated materials from DFT	12
4.2. Phonons and structural stability of elemental Iron	14
5. NONLOCAL CORRELATIONS	17
5.1. DMFT with other extensions of DFT+LDA	17
5.2. Cluster DMFT	17
6. SUMMARY & OUTLOOK	19

1. INTRODUCTION

As early as the first quarter of 20th century, the laws of quantum mechanics were almost completely known, and it was realized that understanding the properties of crystalline matter was in principle a problem of solving the Schroedinger equation for the electrons. In 1929 Paul Dirac, one of the founding fathers of quantum mechanics, published an article titled *Quantum Mechanics of Many-Electron Systems*, in which he famously claimed that (1)

“The general theory of quantum mechanics is now almost complete, the imperfections that still remain being in connection with the exact fitting in of the theory with relativity ideas. (...) The underlying physical laws necessary for the mathematical theory of a large part of physics and the whole of chemistry are thus completely known, and the difficulty is only that the exact application of these laws leads to equations much too complicated to be soluble. It therefore becomes desirable that approximate practical methods of applying quantum mechanics should be developed, which can lead to an explanation of the main features of complex atomic systems without too much computation.”

A plethora of numerical methods were developed in the course of the past century with the aim of achieving an accurate enough solution to the Schroedinger equation for electrons in molecules and solids (2, 3). Those different methods have achieved different levels of success. For example, the Thomas-Fermi Theory, which predates even the quote above, is good for qualitatively explaining total energies of atoms, but cannot predict any chemical bonding (4). The Hartree-Fock approach, on the other hand, is capable of reproducing various chemical phenomena but only at the cost of a much higher computational cost, and fails to capture electronic states that cannot be represented as a single Slater determinant.

The workhorse method for solid state materials physics is the Density Functional Theory (DFT).¹ The state of the art DFT is extremely successful, and reproducible (5); however it

¹The idea of using density as the basic variable and forming a theoretical framework that relies on

also has fundamental shortcomings, such as the absence of dynamic electronic correlations which are important in Mott insulators. The Dynamical Mean Field Theory (DMFT) is an approach that was originally developed to solve the Hubbard model, and it was interfaced with DFT to become first principles DFT+DMFT soon after (6). Its successes include, but are not limited to, the prediction of correct electronic structure for Mott insulators and correlated metals (7). With more and more applications of first principles DFT+DMFT to novel materials systems, this method is no longer used exclusively by the physicists focused on the correlated electronic phases but is now becoming a widely used tool for the materials science community as well (8).

The aim of this brief review article is to use some successful applications of the DFT+DMFT method to demonstrate its capabilities to non-experts. In this respect, it is neither a complete review of the intricacies of this method, nor is it even a nearly complete list of applications of DFT+DMFT. It is rather a short introduction for experimentalists and theorists focused on other approaches, and we refer the reader to many excellent review articles on the fundamentals and applications of this method for further information (9, 10, 11, 12, 7, 13).

This article is organized as follows: In Section 2, we give a very brief background on the DFT and DMFT. In Section 3, we demonstrate how DFT+DMFT can correct the spectra and reproduce the correlation induced mass enhancement in correlated metals. Section 4 demonstrates the DMFT corrections to the crystal structures and phonon spectra of correlated materials. Section 5 provides examples of the extensions of DMFT to include nonlocal correlations. We conclude by Section 6, a summary.

2. DFT, DMFT, and DFT+DMFT

2.1. Density Functional Theory

The starting point of DFT is the observation that the many-electron wavefunction Ψ is a prohibitively expensive function to numerically work with. For N electrons, Ψ is a function of $3N$ variables such as the cartesian coordinates $x_1, y_1, z_1, x_2, \dots, z_N$. The number of bits required to numerically store such a function scales exponentially with the number of electrons N (4), and becomes larger than the number of protons in the observable universe for even relatively humble molecules. This limits the applicability of numerical approaches that rely on brute force calculation of the wavefunction.

One way to circumvent this exponential barrier is to use the electron density ρ , instead of the many-electron wavefunction Ψ . Being only a function of three spatial coordinates, $\rho(x, y, z)$ does not suffer from the same exponential scaling. However, being a real function in a much fewer dimensional space, ρ might seem to hold much less information than Ψ . Nevertheless, the Hohenberg-Kohn Theorem of 1964 (14) states that ρ implicitly carries all the necessary information about the groundstate properties. Citing (4):

“The groundstate density of a bound system of interacting electrons in some external potential

functionals of density is a very general one, and it is possible to construct different DFT approaches. However, the dominant convention in the electronic structure community is to refer to a particular DFT framework, the Kohn-Sham DFT combined with the Local Density Approximation (LDA) or Generalized Gradient Approximations (GGA), as *the* DFT, and throughout this paper, we follow this convention as well.

V determines this potential uniquely.”

In the context of a crystal, the external potential V is the electrostatic potential of the ion cores. Since ρ determines V , it also determines the full electronic Hamiltonian. As a result, the groundstate density ρ carries all the information about the physical system. In other words, there is in principle a functional of density ρ for any physical observable. However, in practice, these functionals are not known, and only approximate DFT calculations are performed.

The Kohn-Sham DFT relies on solving a noninteracting problem instead of the interacting one by defining an effective Coulomb potential V_C that stems from both the external (ionic) potential V , and the electrons

$$V_C(\vec{r}) = V(\vec{r}) + \int \frac{\rho(\vec{r}')}{|\vec{r} - \vec{r}'|} d\vec{r}' \quad (1)$$

and an *exchange correlation functional* V_{xc} . The ground state density $\rho(\vec{r})$ is the solution of the self consistent equations

$$\left(-\frac{1}{2}\nabla^2 + V_C(\vec{r}) + V_{xc}(\vec{r}) - E_i \right) \psi_i(\vec{r}) = 0 \quad (2)$$

and

$$\rho(\vec{r}) = \sum_i |\psi_i(\vec{r})|^2 \quad (3)$$

Here, ψ_i are the wavefunctions for the Kohn-Sham quasiparticles, which are noninteracting. This simplifies the N electron problem to N one-electron problems. This form of the equations is exact, and the Kohn-Sham eigenvalues E_i can be used to calculate the total ground state energy of the system. However, the form of the exchange correlation functional V_{xc} is not known. Even though it is often written as a local function, the value of V_{xc} at \vec{r} depends on the electron density distribution in the whole space. While its overall magnitude is small compared to the Hartree potential V_C , the errors in approximating the exchange-correlation functional can lead to qualitative errors. It is the shortcomings of the present approximations to V_{xc} that makes DFT unreliable in certain types of materials systems.

The simplest approximation to the exchange correlation functional is to assume that it is a local function that only depends on the magnitude of the electron density at point \vec{r} , and it is equal to that of a homogeneous electron gas with equal density. This leads to the so-called local density approximation (LDA). The value of the exchange-correlation energy of the homogeneous electron gas can be calculated numerically with arbitrary precision, as has been done by Ceperley and Alder in 1980 using a Monte Carlo approach (15). LDA is expected to work well in the limit that the electron density changes slowly with \vec{r} , however, what quantity defines the slow change is far from obvious. Nevertheless, DFT with the LDA works surprisingly well for a wide range of systems, including many molecular systems, and crystalline systems such as band insulators or uncorrelated metals. Various Generalized Gradient Approximations that take into account the derivative of the electron density are commonly used to approximate V_{xc} as well (16). While GGAs provide better quantitative results for certain quantities such as the lattice constants or binding energies, they suffer from the same fundamental shortcomings of the LDA.

2.2. Dynamical Mean Field Theory

The large spatial extent of electrons in the s and p orbitals of atoms and the broad energy bands formed by these orbitals in solids facilitate the screening of the intra-atomic Coulomb interaction that is effectively felt by these electrons. These electrons are highly itinerant and their large kinetic energies dominate over the Coulomb interaction. Usually, a static mean field approximation is suitable to describe s and p electrons because their wavefunctions are not strongly correlated, and can be expressed by a single Slater determinant. Band theory, which relies on an independent electron approximation, treats electrons as Bloch waves and is a very successful approach in theoretically understanding the physical properties of simple metals, semiconductors, and band insulators. Success of first principles DFT when applied to these materials, in part, relies on this observation.

In contrast, the Coulomb interaction between electrons in the d or f orbitals is often stronger, as electrons in these orbitals with a smaller radial extent and larger number of angular nodes lead to narrow energy bands that lead to weaker screening. Strongly correlated electronic states that cannot be represented in a single Slater determinant emerge often in these systems, and the band theory fails.²

There are several emergent phenomena and phases induced by the correlations of d and f electrons, and couplings between multiple competing degrees of freedom such as spin, charge, orbital, and lattice (18, 7). Examples of such phenomena, which are beyond a simple band theory, include the high temperature superconductivity in cuprates (19), the colossal magnetoresistance in manganites (20), Mott metal-insulator transitions (21), and the mass enhancement of electrons in heavy Fermion systems. Because of this competition, strongly correlated electron systems are often extremely sensitive to external perturbations such as temperature, pressure, doping and magnetic field (21), which renders them both experimentally and theoretically interesting materials to study.

In the limit of strong interactions, electrons become highly localized on atomic sites, and eventually the solid becomes a Mott insulator. Electrons in the Mott insulating state are better described by an atomic-like theory defined in real space, rather than by band theory in reciprocal space; and as a result the wavevector \vec{k} is no longer a good quantum number. The failure of band theory was first observed in insulating transition metal compounds like MnO and NiO by predicting these to be metallic in the absence of long range magnetic ordering (22, 21, 23). In the regime of intermediate interactions, on the other hand, electrons are not fully localized, and can display features of both Bloch-like bands and localization (such as the quasiparticle bands not being sharp, and emergence of upper and lower Hubbard bands). In this correlated metallic regime, it is necessary to consider both natures of electrons, and use a method that takes advantage of both real and reciprocal spaces. Both band theory and an atomic-like theory fail to explain this particular behavior of electrons alone.

Early work on understanding the correlated electronic structure was focused on the Hubbard model (24, 25, 26), which includes a local Coulomb repulsion U between electrons:

$$\hat{H} = \sum_{ij,\sigma} t_{ij} c_{i\sigma}^\dagger c_{j\sigma} + U \sum_i n_{i\uparrow} n_{i\downarrow}. \quad (4)$$

²In principle, since the many-body electronic wavefunction is antisymmetric, any electronic state is correlated. However, a correlated electronic state is usually defined as one that cannot be represented by a single Slater determinant, and correlation effects are defined as those that stem from this fact (17). Often, effects not captured by DFT are also referred to as correlation effects, though this usage can be misleading.

Here, $c_{i\sigma}^\dagger$ and $c_{i\sigma}$ are the creation and annihilation operators associated with the electron with spin σ at i^{th} lattice site, and t_{ij} is the inter-site hopping amplitude. In the $t \gg U$ limit, electrons are itinerant and the band theory works well. In the $U \gg t$ limit double occupation of a site is energetically unfavorable, and the system becomes a Mott insulator at half filling. (The large electron scattering at the Fermi level introduces a gap separating the upper and lower Hubbard bands.) A static mean field theory like Hartree-Fock or DFT cannot capture the dynamic (frequency dependent) correlations that emerges from the strong interactions and scattering between the electrons, and thus cannot predict this Mott insulating state. Dynamical correlations are important in the $t \sim U$ regime as well. In this regime, the width of the quasiparticle band is renormalized, the quasiparticles attain a finite life time (the bands become partially incoherent), and upper and lower Hubbard bands emerge.

The one-band Hubbard model is exactly solvable in one dimension (27) but not in 2 or 3 dimensions (27, 28, 18). As the number of lattice sites increases, the Hilbert space expands exponentially and the many body problem becomes computationally intractable even in modern day supercomputers (18). As early as the 1980s, it was realized that the Hubbard model is more tractable in the limit of infinite dimensions (29) where the electronic self energy becomes independent of the wavevector \vec{k} (30). Subsequently, Georges and Kotliar formulated the idea of mapping the Hubbard model in the infinite dimensional limit into a self consistent single site quantum impurity model, and hence laid the foundations of the dynamical mean field theory (DMFT) approach (31, 12). This non-perturbative approach has directed towards significant advancement in understanding strongly correlated systems (18, 7, 12, 32, 33, 9, 31, 34). DMFT can be considered as an analogue of a classical mean field theory for a ferromagnetic system: The classical and static mean field theory for the magnetic system introduces a magnetic field that is induced by the average magnetization of the whole crystal acting on each magnetic atom. The magnetic configuration of the atom and the mean magnetic field acting on it are determined self consistently. In a similar vein, DMFT replaces the many-body system with a single impurity atom which is embedded in a bath of uncorrelated electrons, and determines the hybridization between the impurity and the bath self consistently. A major strength of this approach is the possibility to treat the quasiparticle and Hubbard bands equally (9, 7).

In DMFT, the many-body problem is mapped onto the well known Anderson impurity model (AIM), which is often used to model magnetic impurities embedded in metals (35, 7):

$$\mathcal{H}_{AIM} = \mathcal{H}_{atom} + \sum_{\nu,\sigma} \epsilon_\nu^{bath} n_{\nu,\sigma}^{bath} + \sum_{\nu,\sigma} (V_\nu c_{0,\sigma}^\dagger a_{\nu,\sigma}^{bath} + H.C.). \quad (5)$$

In this Hamiltonian, \mathcal{H}_{atom} represents the energy associated with the atomic degrees of freedom at the impurity site, ϵ_ν^{bath} are the energy levels of the bath of noninteracting electrons, $n_\sigma = c_\sigma^\dagger c_\sigma$ is the density of electrons with spin σ , and V_ν is the probability amplitude of an electron being exchanged between the impurity and the bath. The frequency dependent hybridization function $\Delta(\omega)$ is defined by V_ν as (7)

$$\Delta(\omega) = \sum_\nu \frac{|V_\nu|^2}{\omega - \epsilon_\nu^{bath}}. \quad (6)$$

The dynamic quantity $\Delta(\omega)$ serves as the dynamical mean field in DMFT, and is the analogue of the Weiss mean field in classical mean field theory of magnetism. The hybridization

function determines the ability of electron to hop in and out of the impurity site. The electrons become localized or itinerant for small and large values of Δ respectively.

The DMFT method can be compared with DFT as shown in Fig. 1a (36). DFT at the level of LDA approximation models the electrons in the real material by non-interacting Kohn-Sham quasiparticles. The exchange correlation energy is calculated by using a model of a homogeneous electron gas with the same density as $\rho(\vec{r})$. DFT+GGA uses derivatives of the charge density $\rho(\vec{r})$ as well, but the model that the system is mapped onto is nevertheless featureless. DMFT is significantly more involved, and considers an impurity atom, such as a transition metal ion with, with all its internal degrees of freedom. The interactions of the impurity atom with an uncorrelated bath of electrons are taken into account via the hybridization function $\Delta(\omega)$. The information about the real material that is retained in the AIM is this hybridization function, which is considerably larger than the information carried by the local electron density alone.

2.3. First Principles DFT+DMFT

DMFT applied to the Hubbard Model led to great advancements in the understanding of the behaviour of the strongly correlated systems, and the nature of phenomena such as the Mott transition. However, DMFT is blind to chemistry: in order to apply DMFT to real materials, it needs to be interfaced with a first principles method like DFT. This is achieved by performing a DFT calculation, and then defining the atoms with d or f electrons as the impurities in the AIM. First attempts to perform DFT+DMFT followed the procedure of building a tight binding model using the first principles calculations, and using the DMFT approach to solve the tight binding model. The most common approach to obtain the first principles tight binding model is to use the maximally localized Wannier orbitals (37). The shortcoming of this ‘one-shot’ approach, however, is that the orbitals that define the DMFT problem are built using a method that does not take into effect the electronic correlations (DFT). It is possible to include the effect of the correlations as given by DMFT on the charge density by repeating the DFT calculation while taking into account the charge density updated by DMFT (38), and almost all modern implementations employ such a self-consistent DFT+DMFT loop. (This, of course, comes with an increased computational cost.) There are also projector-based approaches, which do not suffer from the errors introduced by the Wannierization procedure, such as the possible change of the extent of the orbitals which affects the effective on-site interaction strength (39).

In a typical DFT calculation, the Kohn-Sham wavefunctions, electron density, and the Kohn-Sham Hamiltonian are determined self-consistently, as shown in Fig. 1b. This DFT loop also exists in its entirety in the flow-chart for a DFT+DMFT calculation, a simplified version of which is shown in Fig. 1c. The Kohn-Sham wavefunctions are used to calculate the Green’s function, which in turn determines the impurity hybridization function $\Delta(\omega)$. Solving the impurity problem, computationally the most expensive step, gives the impurity self energy $\Sigma(\omega)$. The self energy updates the Green’s function, which can be fed back to the DFT loop to update the charge density. A typical calculation involves going over both the DFT and DFT+DMFT loops many times to reach self consistency.

The DFT+DMFT approach is now well developed and tested enough to have predictive capabilities, and is used extensively on materials science problems (8, 40). However, like any other method, it still has room for technical improvements. One of the most important problems of DFT+DMFT method is considered to be the double-counting (DC) issue, which

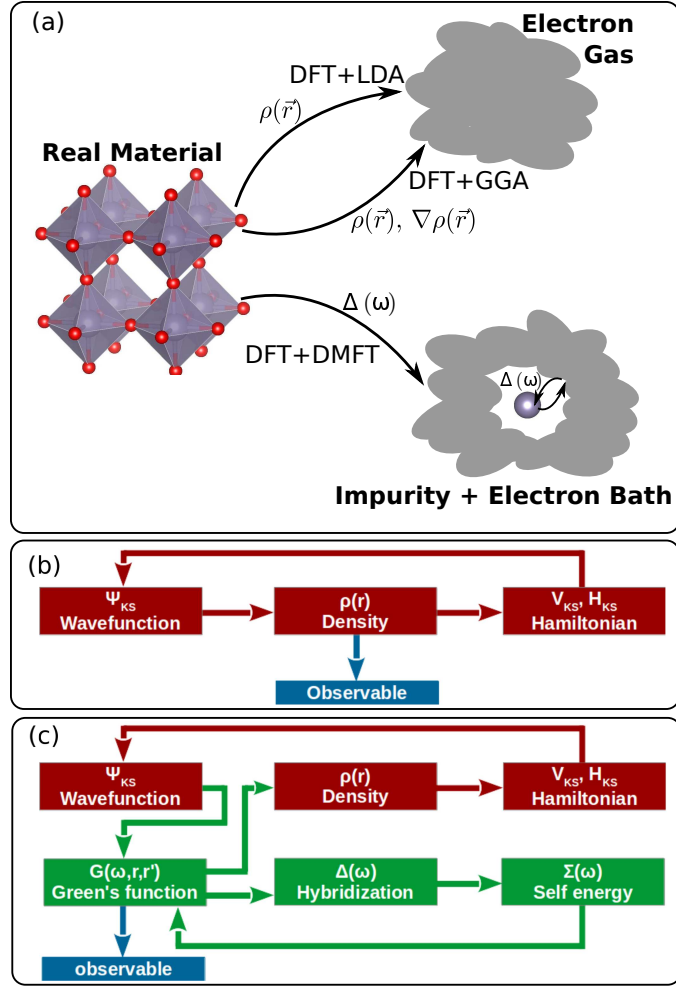


Figure 1

(a) The LDA approximation maps the electronic system to a homogeneous electron gas. In contrast, DMFT maps the system to an impurity that interacts with an electron bath via the hybridization function $\Delta(\omega)$. (b) Typical DFT implementations calculate the Kohn-Sham wavefunctions, electron density, and the Kohn-Sham Hamiltonian iteratively until self consistency is reached. The observables of interest are in principle determined by the electron density. (In practice, the Kohn-Sham wavefunctions are also used.) (c) Typical DFT+DMFT implementation, in addition to performing the DFT iterations, involves calculating the Green's function, Hybridization $\Delta(\omega)$, and the electronic self energy $\Sigma(\omega)$.

arises in any electronic structure method that incorporates additional interaction terms onto DFT (41, 42). As DFT includes a certain part of the static correlations of electrons through the exchange-correlation functionals (LDA or GGA), it is necessary to subtract the part of energy that is accounted for twice. This double counted part of the correlation energy shifts the energies of correlated states with respect to the uncorrelated ones, and can give rise to errors in the final electronic structure: for example, the $p-d$ charge transfer energy of

transition metal oxides often depend on the choice of DC scheme (43). Historically, simple expressions for the DC energy were borrowed from the DFT+U literature, and this problem was one of the most common reasons used to claim that DFT+DMFT is not a true first principles method (36). The two prevalent approaches were the “Fully Localized Limit” (44) and the “Around Mean Field” (41) formulas. However, these formulas often need to be ‘tuned’ with only a posteriori justification (45). A recent development on the DC problem is the derivation of an exact DC expression using a continuum representation of DMFT (46). This approach takes into account the nonsphericity of the impurity, and has so far produced good agreement with the experiment (36, 47), possibly concluding the discussion over the different DC approaches.

Another area where there is need for new developments is the numerical impurity solvers, which solve the AIM to calculate the self energy $\Sigma(\omega)$ from the hybridization $\Delta(\omega)$ (8). The state of the art is the continuous time quantum Monte Carlo methods introduced for this purpose (48, 49, 50) which are in principle exact, and efficiently parallelizable over a large number of processors. However, their applicability is strongly limited by the computational cost for large number of impurity orbitals, and reduced Monte Carlo noise. New algorithmic developments, such as the ‘lazy skip lists’ are introduced to reduce the computational needs (51), but applications of state of the art DMFT on problems with large impurities, such as certain f electron compounds, and clusters of transition metals, are still hardly within reach except for large scale supercomputers.

3. MASS RENORMALIZATION IN CORRELATED METALS

How the inclusion of electronic correlations at the DMFT level changes the DFT band structure can be illustrated by considering the electronic Green’s function $G(\vec{k}, \omega)$, which is the fourier transform of the electron propagation amplitude. For a one-band system:

$$G(\vec{k}, \omega) = \frac{1}{\omega - E(\vec{k}) - \Sigma(\omega, \vec{k})} \quad (7)$$

Here, $E(\vec{k})$ is the energy of the band at \vec{k} according to DFT, and $\Sigma(\vec{k}, \omega)$ is the self energy obtained from the DMFT calculation. If $\Sigma=0$, the Green’s function has poles at $\omega = E(\vec{k})$, and the spectral function

$$A(\vec{k}, \omega) = -\frac{1}{\pi} \text{Im}(G(\vec{k}, \omega)) \quad (8)$$

consists of a Dirac delta for each \vec{k} at $\omega = E(\vec{k})$. Hence, the spectral function is equivalent to the DFT band structure.

The self energy $\Sigma(\omega, \vec{k})$ is in general a complex function of frequency and the wavevector \vec{k} , and is well behaved for weakly correlated systems such as band insulators or metals that behave as Landau Fermi liquids. Its real part shifts poles in the spectral function from the band energy $E(\vec{k})$, and its imaginary part broadens the poles, which are no longer Dirac deltas. (This corresponds to a finite quasiparticle life time due to electron-electron scattering.)

The single site DMFT approximation, which assumes that the correlations are local to a single atomic site and works for a multitude of transition metal oxides, leads to a self energy $\Sigma(\omega)$ has no \vec{k} dependence. $\Sigma(\omega)$ has a simple form in metals that behave as a Landau Fermi Liquid. Near the Fermi level, the imaginary part of Σ goes to zero quadratically since the quasiparticles are long lived, and the real part of Σ becomes a linear function of ω . It is

still possible to speak of a bandstructure with well defined bands, since the imaginary part of Σ is zero, but the bandwidth is narrower than the DFT bandwidth by a factor of

$$Z = \frac{1}{1 - \frac{d\text{Re}(\Sigma)}{d\omega}} \quad (9)$$

The reciprocal of Z can be considered as a mass renormalization factor, since the electron effective mass calculated from DFT (often referred to as the *band mass*)

$$m_{\text{band}}^* = \hbar^2 \left(\frac{\partial^2 E(k)}{\partial k^2} \right)^{-1} \quad (10)$$

is smaller than the mass approximated from the DMFT spectral function by a factor of Z

$$m_{\text{DMFT}}^* = Z^{-1} m_{\text{band}}^* \quad (11)$$

A compound with no electronic correlations that cannot be captured by DFT at the LDA level has $Z = 1$. Stronger electronic correlations lead to a smaller Z , which approaches zero as one approaches the Mott insulating phase in the phase diagram.

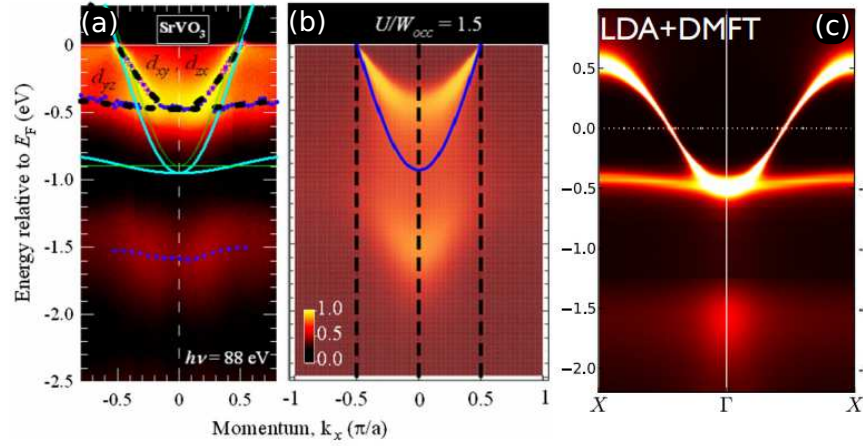


Figure 2

ARPES and first principles results for the spectral function of correlated metal SrVO₃. (a) ARPES spectral weight from Ref. (52). The dark blue dots are a fitted tight binding model, and the light blue lines are the DFT bands. (b) Spectral function from the one-band DMFT calculation from Ref. (52). Dark blue line is the uncorrelated band structure used as the input to the DMFT calculation. (c) Results of the self consistent DFT+DMFT calculations from Ref. (53). Copyright (2009) and (2015) by the American Physical Society.

The cubic perovskite oxide SrVO₃ (54) provides a clear illustration of this point. This compound has a simple band structure with only partially filled t_{2g} bands of V crossing the Fermi level. Angle-Resolved Photoemission Spectroscopy (ARPES) measurements of Takizawa et al. (52) show that these t_{2g} bands are relatively coherent (are not broadened very much by the imaginary part of the self energy), as reproduced in Fig. 2a. The bandwidth predicted by DFT calculations, displayed as the blue lines superposed with the ARPES result, is larger by about a factor of 2.

In order to correct the bandwidth, Takizawa et al. performed a DMFT calculation on a one-band model (52). This model calculation considered a tight binding model that was obtained from the first principles DFT calculation, but it did not take into account all the bands present in the material. Nevertheless, this calculation provides significant improvement over the DFT band structure. For the on-site interaction U set to 60% of the uncorrelated bandwidth W , $U = 0.6W$, Takizawa et al. found $Z \sim 0.5$ which gives the correct bandwidth for the quasiparticle band (Fig. 2b). However, this one band approach overestimates the dispersion of the incoherent satellite at -1.5 eV that consists of the spectral weight transferred from the coherent band. This is possibly due to the omission of the other t_{2g} bands that overlap (52). LDA+DMFT calculations that don't omit the other t_{2g} bands, such as the early calculations by Nekrasov et al. that employ a downfolding scheme and considered 3 correlated t_{2g} orbitals per V ion, also reproduce a similar Z value (55). Relatively recently, a fully charge self consistent DFT+DMFT calculation performed by one of us (Birol) and Haule (53) correctly reproduced not only the Z factor of $Z \sim 0.5$, but also the weakly dispersive satellite at -1.5 eV (Fig. 2c).

The reason that one can easily define a band structure and observe sharp bands in SrVO₃ is that it is only a mildly correlated metal. The heavy fermion compounds, by comparison, are extremely correlated Fermi liquid systems, and the effective mass of electronic quasiparticles in these compounds can be multiple orders of magnitude larger than in ordinary metals, or what DFT predicts for them (56). In these systems, the Fermi step is reduced from its uncorrelated value 1 so much that the observation of a Fermi surface and measuring a Z (which is typically $\sim 0.01 - 0.001$) is very hard. An easy way to detect the signature of the very strong correlations in heavy fermion compounds is the anomalously large electronic specific heat Sommerfeld coefficient γ in these systems

$$C_e = \gamma T \quad (12)$$

which is also renormalized with respect to its DFT value by the same amount as the effective mass (57).

$$\frac{\gamma}{\gamma_{band}} = \frac{m_e^*}{m_{band}^*} \quad (13)$$

DFT+DMFT approach has been extensively used to study heavy fermion compounds as well. For example, LiV₂O₄, a frustrated, mixed valence spinel (58) that exhibits the largest specific heat enhancement among the heavy fermion compounds that don't contain a rare earth ion (59), has been studied by Arita et al., who showed that there is a very sharp (heavy) quasiparticle peak near the Fermi surface (60). Haule et al. (39, 61) studied the 115 heavy fermion materials CeIrIn₅, CeCoIn₅, and CeRhIn₅. Comparing the characters of the Ce f electrons as obtained from DMFT shows that the localization tendency is highest in CeRhIn₅, and the electrons in the Iridium compound CeIrIn₅ display the most itinerant character; both in line with the experimental observations. Later work by Choi et al. (62) showed that the electronic temperature directly affects the Fermi surface in these 115 compounds. Even though DFT correctly reproduces the shape of the low temperature Fermi surface, it does not contain any temperature for the electrons. The DMFT calculation, on the other hand, naturally includes the electronic temperature and hence allows studying the evolution of the Fermi surface with temperature (Fig. 3).

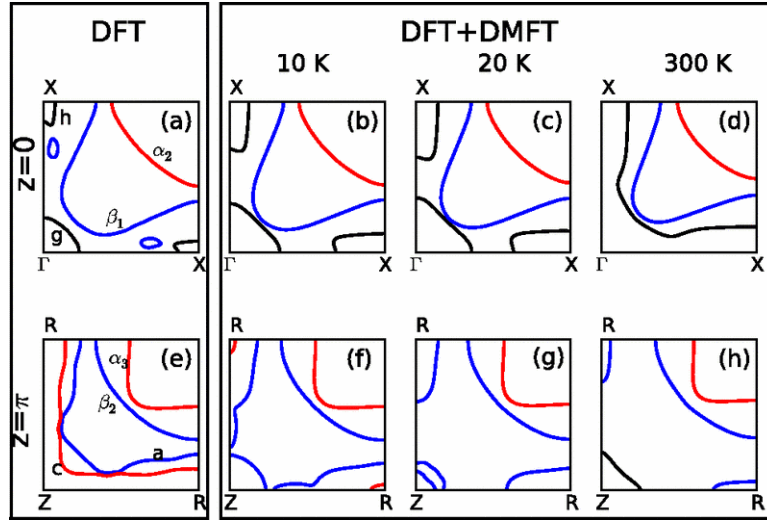


Figure 3

Cuts through the Fermi surface of CeIrIn_5 at different k_z values from DFT and DFT+DMFT. The DFT+DMFT approach allows performing the calculation at different temperatures to elucidate temperature evolution of the Fermi surface. Reproduced from Ref. (62). Copyright (2012) by the American Physical Society.

4. CRYSTAL STRUCTURES AND LATTICE RESPONSE FROM DFT+DMFT

4.1. Error in lattice parameters of correlated materials from DFT

DFT has evolved considerably since the original theorems of Kohn et al. (14, 63). Part of this evolution was a transition from in-house codes written and maintained by small groups to large scale packages used by thousands of groups that increased precision and reproducibility (5). Interestingly, the simplest approximation to the exchange-correlation energy, the so-called local density approximation (LDA) that was originally proposed by Kohn et al. in References (14, 63), is still commonly used. LDA is surprisingly accurate in predicting crystal structures of band insulators and uncorrelated metals (64). It is well known to underestimate the lattice constant by $\sim 1\%$ because it does not assign an energy cost to a larger electronic density gradient, but there is no obvious reason why the error of such a simple approximation should be this small. Various generalized gradient approximations (65) give even better results than LDA. For example, the PBEsol functional is developed specifically for solids (66, 67) and it often has an error of the order of few tenths of a percent for the lattice parameters (68). Other details of the crystal structure (the positions of the atoms in the unit cell) and linear response properties such as phonon frequencies can also be precisely determined in band insulators using either LDA or its simple extensions (64). Historically, these methods provided significant levels of insight and quantitative accuracy in the study of crystallographic phase transitions, the best example being the ferroelectric transitions in oxides (69, 70).

In certain compounds, such as the Mott-insulating 3d transition metal oxides, LDA often underestimates the lattice parameters with a much larger error margin. For example, performing a DFT calculation without magnetic ordering leads to an underestimation of the

lattice constant of FeO by $\sim 7.7\%$ by LDA and $\sim 5.1\%$ by PBE (a type of GGA) compared to the experimental value in the paramagnetic state (53). (PBE usually tends to *overestimate* lattice constants in band insulators.) Performing the calculation with antiferromagnetic order reduces the error and leads to an underestimation of $\sim 3.6\%$ and $\sim 0.7\%$ by LDA and PBE respectively. While this is a smaller error, it is nevertheless significantly higher than that in the results obtained for band insulators, pointing to the presence of a physical reason that leads to enhanced overbinding of the lattice in compounds like FeO.

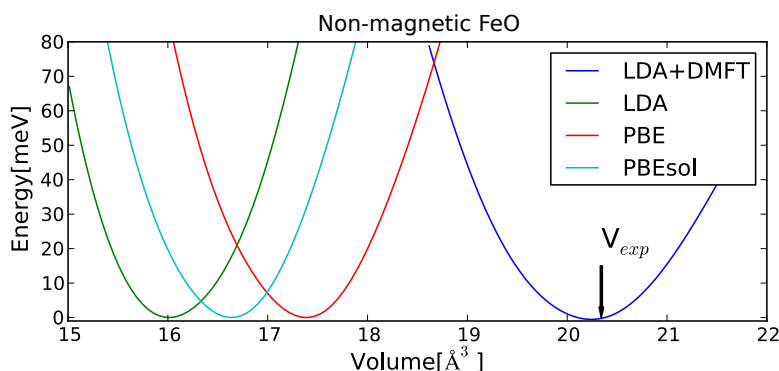


Figure 4

Energy as a function of unit cell volume for cubic FeO without magnetic order, calculated using DFT with LDA (green), PBE (red) and PBEsol (light blue) exchange correlation functionals, as well as DFT+DMFT (dark blue). The minimum of the energy gives the predicted volume. The black arrow denotes the experimentally observed value V_{exp} . Reproduced from Ref. (53). Copyright (2015) by the American Physical Society.

A major reason for the underestimation of the lattice constant, especially in nonmagnetic DFT calculations, is the strong underestimation of the local magnetic moments by DFT at the LDA or GGA level. The paramagnetic state often involves large local, atomic magnetic moments. For example, in a transition metal cation with 4 valence electrons under a cubic crystal field, all of the electrons often have parallel spin due to atomic Hund's coupling (Fig. 5a) even in the paramagnetic phase. In the absence of magnetic order, the atomic magnetic moment is fluctuating, and $\langle S_z \rangle = 0$, even though $\langle S_z^2 \rangle \neq 0$. Kohn-Sham DFT cannot directly capture this phase, and a simple DFT calculation without magnetic ordering simulates a state where $\langle S_z \rangle = 0$, and $\langle S_z^2 \rangle = 0$. This often corresponds to the low-spin configuration in Fig. 5b.

The underestimation of the lattice constants by LDA/GGA can to a large extent be explained by the absence of a local, fluctuating magnetic moment. In an oxide like FeO, the bonding of a high-spin cation with an electron in the higher lying e_g orbitals (Fig. 5a) is in general very different from that of a low-spin cation without any electrons in the e_g shell. This is because of the fact that e_g orbitals are extended towards the oxygen anions, and are σ bonding with them (71). Electrons on the e_g orbitals strongly repel the oxygen anions, and hence favor a larger lattice constant. A nonmagnetic DFT calculation that places all the electrons to the lower lying t_{2g} orbital strongly favors an underestimated lattice constant. In addition to the large errors in lattice parameters, the phonon spectra that DFT predicts for these compounds are often both quantitatively and qualitatively wrong. Imposing a magnetic order in LDA fixes part of the error, but is often not enough

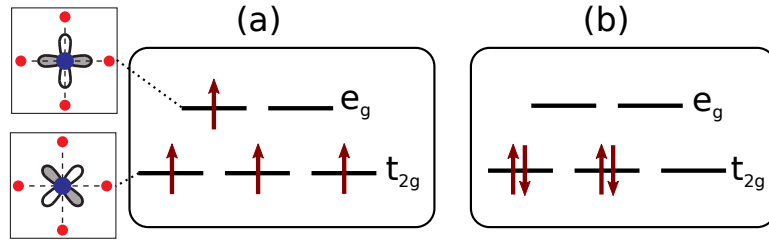


Figure 5

Sketch of the atomic energy levels and the electronic configuration of a transition metal with 4 electrons on its d shell, under a cubic crystal field. (a) The high-spin configuration, where the higher e_g states, which have lobes extended towards the oxygen anions, are partially occupied. (b) The low-spin configuration, where only the lower t_{2g} orbitals without lobes extended towards oxygens are occupied.

to fix all of it, since obtaining a realistically large ordered moment in transition metal oxides often requires the correction of the on-site Coulomb interaction by a Hubbard-U term as well (41, 72, 73). Also, in many compounds such as in the stripe-type antiferromagnetically ordered iron pnictides, the antiferromagnetic order breaks lattice symmetries in addition to the time reversal symmetry (74). In these systems, the antiferromagnetic state does not provide a good approximation to the paramagnetic phase for calculating crystal structure properties. DFT+DMFT approaches, on the other hand, bring the capability to perform calculations in a truly PM phase, with nonzero local fluctuating moments, as well as ordered moments. This, in addition to the dynamical correlations that DMFT introduces, has been recognized early on as a means to correctly reproduce the lattice parameters and phonon spectra of correlated materials from first principles. The result of the calculation of lattice parameter of paramagnetic FeO by DMFT, displayed in Fig. 4, exemplifies this point.

4.2. Phonons and structural stability of elemental Iron

Early examples of work on the structural stability and response of correlated materials include the study by Savrasov et al. (75) on the phonon band structure of MnO and NiO, and the work of Dai et al. (76) which reproduced not only the phonon spectra but also explained the unusually large anisotropy in the elastic properties of this compound (76). Both of these studies employed the Hubbard-I approximation (25) to solve the DMFT impurity problem. (The Hubbard-I approximation does not give as precise results as the state of the art Monte Carlo approaches, but it is computationally much cheaper and does not require the relatively delicate analytical continuation step.) DFT+DMFT approach also made important contributions to applied problems, for example by explaining the low thermal conductivity of nuclear fuel materials UO_2 and PuO_2 (77).

Even one of the oldest materials known to mankind, elemental iron, is not exempt from electronic correlation effects. It was recognized early on that even though elemental metals have seemingly large bandwidths, the 3d transition metals also have large on-site Coulomb interactions, and hence their electronic and magnetic properties are more correctly given by a DFT+DMFT treatment than by DFT alone (78, 79, 9, 80). As a function of temperature, elemental iron undergoes multiple phase transitions before melting. Fe is a ferromagnet with a body-centered cubic (BCC) crystal structure (α -phase) at low temperature. The crystal

structure becomes face-centered cubic (FCC) at ~ 1185 K, just ~ 140 K above Curie temperature at which the ferromagnetic order disappears (γ -phase); but it becomes BCC again at ~ 1670 K (δ -phase), close to its melting temperature. Nonmagnetic DFT calculations predict strong lattice instabilities (imaginary phonon frequencies) for both the α and the γ structures, which poses a clear contradiction with the experimental observations. Leonov et al. employed a Wannier based DFT+DMFT approach and the Hirsch-Fye algorithm for the impurity solver (81) to address the structural stability of Fe near its phase transitions (82, 83, 84), and reached the conclusion that “electronic correlations determine the phase stability of iron up to the melting temperature” (84).

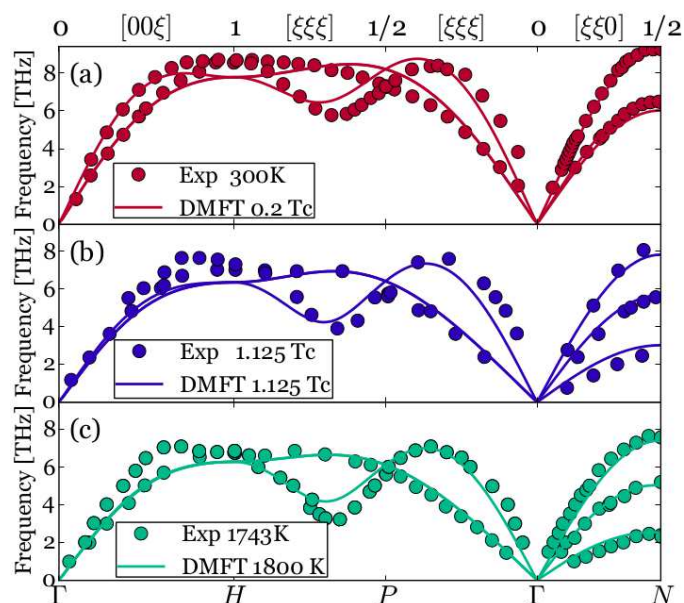


Figure 6

Phonon dispersions of elemental iron (a) at the ferromagnetic α phase, (b) at the α phase with magnetic order at higher temperature, and (c) at the δ phase. Reproduced from Ref. (85). Copyright (2018) by the American Physical Society.

In Fig. 6, we present the phonon dispersions of iron at different phases and temperatures, reproduced from Ref. (85) by Han, Birol, and Haule. The DFT+DMFT approach that we used in this work is fully charge self consistent, and uses the numerically exact Continuous Time Quantum Monte Carlo (CTQMC) impurity solver (49, 39). In order to overcome the Monte-Carlo numerical noise in the calculations, in addition to good statistics (which comes at the cost of high computational cost), a stationary implementation of DFT+DMFT is necessary. The stationary implementation we used (53) allows the calculation of the free energy (including the electronic entropy) and accurate forces on the atoms (86, 36). This implementation of the forces also takes into account the electronic entropy, which can be particularly important near a Mott or spin state transition. (For example, LaCoO_3 displays both a spin-state transition and anomalous thermal expansion (87); and the high temperature crystal structure is energetically favorable only when the electronic entropy is taken into account in DFT+DMFT (88).)

Our results show that iron is dynamically stable at all temperatures in all of its phases; in other words, the fully charge self-consistent DFT+DMFT calculations do not predict any unstable phonons at any temperature or structure. This result explains the reason behind the phonon softening observed near T_C (89) as merely the melting of the magnetic order, and not the proximity to the $\alpha \rightarrow \gamma$ structural transition. The total energy along the Bain path (the path that involves both strain and ionic displacements, and connects the BCC and FCC structure (90)) has two local minima corresponding to FCC and BCC at all temperatures, but the relative energy of these minima change as the system crosses the structural transition temperature (Fig. 7). This is a surprising result that goes against the common assumption that the softening observed near the magnetic transition is a precursor of the martensitic transition (91), and demonstrates the power of the DFT+DMFT approach in providing insight on the coupling between crystal structure and correlated electronic phases.

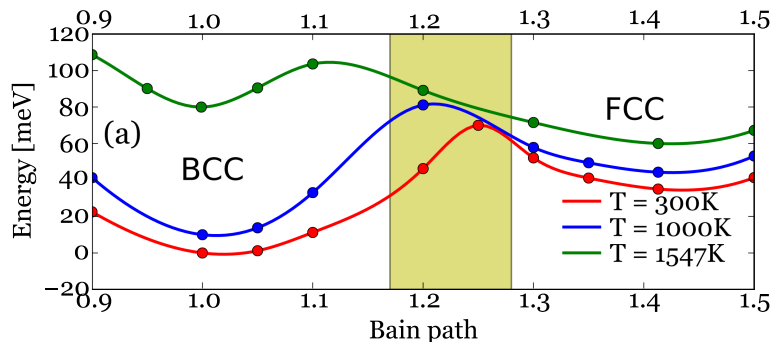


Figure 7

The free energy of elemental iron along the Bain path as obtained from DFT+DMFT at different temperatures. Reproduced from Ref. (85). Copyright (2018) by the American Physical Society.

While it is not possible to simulate a paramagnetic phase directly within DFT+LDA, it is possible to approximate certain properties of materials in the paramagnetic phase using only DFT+U by employing a multi-step approach and constructing multiple large supercells with different magnetic configurations. For example, the *special quasirandom structures*, which originally emerged from studies of alloys (92), were recently used to study MnO, FeO, CoO, and NiO by Trimarchi et al. (93). A similar method was also used by Körmann et al. to calculate the phonon spectra of paramagnetic iron (94), which lead to studies of pressure dependence of phonons, and magnon-phonon coupling in this system (95, 96). Other groups employed a similar approach to study the temperature dependence of phonons in Earth's core conditions (97) and near the γ - δ phase transition (98) with the help of an auxiliary Heisenberg magnetic model used to simulate the magnetic state at nonzero temperature. While all of this work provides valuable insight, the idea of replacing a fluctuating moment in a paramagnet with a spatial disorder of magnetic moments, which relies on ergodicity (85), falls short of simulating the dynamic fluctuations at finite temperature.

Other examples of DFT+DMFT studies on the coupling between the electronic correlations, and the crystal structure and response of correlated materials include the work of Kuneš et al. on the pressure induced volume collapse and metallization of MnO (99), the Jahn-Teller effect in KCuF_3 (100), and the extensive work on rare earth nickelates, including the explanation of the site selective Mott transition in these compounds (101, 102).

These last two examples point out to the success of DFT+DMFT in studying structural phase transitions in correlated materials.

5. NONLOCAL CORRELATIONS

5.1. DMFT with other extensions of DFT+LDA

While single site DMFT corrects the shortcomings of DFT+LDA by adding dynamical correlations that are local to an atom, it is not always sufficient for correctly reproducing the properties of materials where nonlocal correlations (either static or dynamic) beyond LDA are important. An example of such a compound is Cerium(III) Oxide Ce_2O_3 (103). Hybrid functionals that are now commonly used in DFT studies include the nonlocal Fock exchange (104, 105, 106, 107, 108, 109, 110) and correctly predict Ce_2O_3 to be an insulator (111). They additionally improve lattice properties significantly with respect to LDA (111), but they do not reproduce the dynamically correlated 4f Hubbard bands correctly in the paramagnetic state. A natural approach to bring together the best of both hybrid functional and DMFT methods is taken by Jacob et al. (112), who performed a DFT + Hybrid Functional + DMFT calculation on Ce_2O_3 . In this approach, the exact exchange included in the hybrid functional corrects the magnitude of the Cerium d - Oxygen p gap, and the single site DMFT corrects the dynamically correlated Cerium f states.

Another approach, which can be used to take into account the screening by long-range Coulomb interactions, involves combining GW with DMFT. The GW approach is known to produce impressive results in semiconductors (113), and attempts to interface it with DMFT were undertaken as early as early 2000s (114, 115). Modern applications of GW+DMFT to the correlated metal SrVO_3 show that while the dynamical renormalizations are essentially local to the vanadium ion in this compound, the nonlocal correlations screen the Fock exchange and dramatically modify the unoccupied states (116, 117). Some correction to the position of the lower Hubbard band is also reported in SrVO_3 (118). On a completely different type of materials, Hansmann et al. applied the GW+DMFT to effective Hamiltonians obtained from first principles calculations of Si(111) surface with adatoms such as Sn, Si, C, and Pb, and verified the expectation that the nonlocal effects are particularly important in charge density wave systems (119). Another recent development in GW+DMFT is the implementation of first principles quasiparticle self-consistent GW + DMFT (QSGW+DMFT) (120).

5.2. Cluster DMFT

It is possible to explicitly prove that nonlocal dynamic correlations are not important for a particular class of compounds. For example, Semon et al. (121) considered a model that represents the iron pnictide and chalcogenide superconductors and showed that it is justified to use single-site DMFT for these compounds. On the other hand, there are compounds such as VO_2 , where nonlocal dynamic correlations are essential. VO_2 is a metal and has the tetragonal rutile structure above ~ 340 K (Fig. 8a). In this structure, the vanadium cation is in the center of an oxygen octahedron. The octahedra are corner sharing in two dimensions, but are edge sharing along the crystallographic c axis. These edge sharing octahedral chains lead to a smaller distance between the nearest neighbor cations, which results in direct V-V interactions, studied in detail for many decades (122). One of the t_{2g} orbitals of the V cation has lobes pointing along the direction of the edge-sharing

octahedral chains. This orbital has overlap with the nearest neighbor V cations (Fig. 8b), and is responsible for coincident metal-insulator and monoclinic dimerization transitions observed at 340 K (Fig. 8c). The nature of this transition, in particular whether the low temperature phase is a Peierls or a Mott insulator has been the subject of debate.

Both DFT (123) and DFT+(single site)DMFT calculations predict a metallic phase in the monoclinic structure (124), which is not in line with the experimental observations. In order to take into account the nonlocal correlations, Biermann et al. (125) performed cluster DMFT (C-DMFT) calculations on the Wannier functions obtained from DFT. In C-DMFT, the impurity is considered to consist of more than one V atoms, and hence correlations that are not local to an atom can also be included in the DMFT self energy. While this approach increases the computational cost significantly (due to multiple reasons including the larger number of orbitals in the impurity), it is necessary for taking into account dynamical nature of the nonlocal correlations. Biermann et al.’s calculations reproduced the insulating monoclinic phase, and showed that “dynamical V-V singlet pairs due to strong Coulomb correlations is necessary” for the formation of the Peierls gap in VO₂. Lazarovitz et al.’s similar calculations on a downfolded model addressed the effect of strain on the monoclinic transition (126). Recent first principles, self consistent DFT+DMFT calculations (127, 128) support this picture, and emphasize the importance of nonlocal correlations both in VO₂, and its less correlated cousin NbO₂.

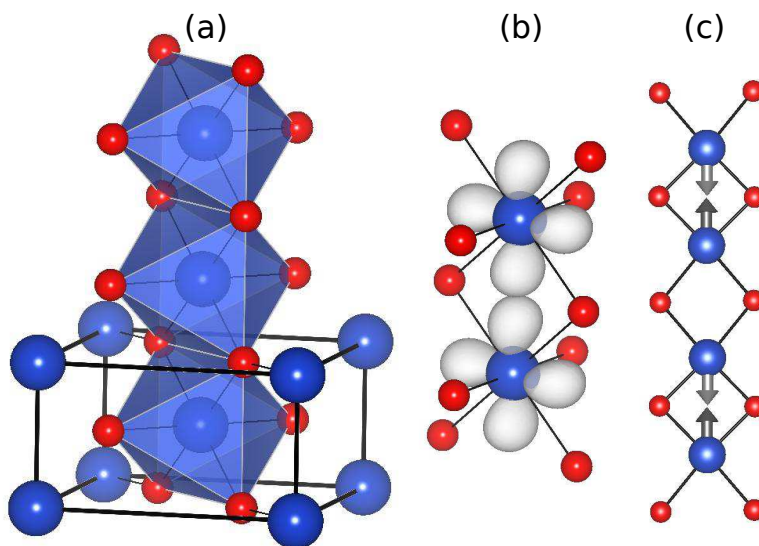


Figure 8

(a) The Rutile crystal structure of VO₂ at high temperature. The tetragonal crystallographic unit cell consists of two formula units, with two V ions on the corner and the body center of the cell. The oxygen octahedra surrounding the V cations form edge-sharing chains along the crystallographic c axis. (b) One of the t_{2g} orbitals on each V ion has lobes extended along these octahedral chains, enabling significant direct V-V hopping of electrons. (c) Below 340 K, V ions along each chain dimerize and lower the symmetry to monoclinic.

6. SUMMARY & OUTLOOK

2019 marks 20 years since Franceschetti and Zunger introduced the *inverse bandstructure problem* of finding out what compound gives rise to a desired functionality (129). In the two decades since, first principles DFT has been extremely successful in not just explaining and supporting experimental observations, but also providing predictions and guiding the experiments in new directions and to new materials.

This procedure, often dubbed *materials by design*, is however limited by the theoretical tools available, in particular, the shortcomings of DFT. The method reviewed in this article, first principles DFT+DMFT, is a leading tool that can to a good extent correct the errors of DFT when applied to correlated materials. Recent developments in the methodology, and implementations of DMFT are now enabling a larger community to work on new problems, and come up with verifiable predictions. These developments have finally turned *correlated materials by design* into reality, and more insight and predictions from DFT+DMFT are sure to follow (40).

DISCLOSURE STATEMENT

The authors are not aware of any affiliations, memberships, funding, or financial holdings that might be perceived as affecting the objectivity of this review.

ACKNOWLEDGMENTS

This work was supported by the NSF-DMR under grant DMREF-1629260. We acknowledge useful discussions with Onur Erten.

LITERATURE CITED

1. Dirac PAM. 1929. Quantum mechanics of many-electron systems. *Proc. R. Soc. Lond. A* 123:714–733
2. Szabo A, Ostlund NS. 2012. Modern quantum chemistry: introduction to advanced electronic structure theory. Courier Corporation
3. Martin RM. 2004. Electronic structure: basic theory and practical methods. Cambridge university press
4. Kohn W. 1999. Nobel lecture: Electronic structure of matterwave functions and density functionals. *Reviews of Modern Physics* 71:1253
5. Lejaeghere K, Bihlmayer G, Björkman T, Blaha P, Blügel S, et al. 2016. Reproducibility in density functional theory calculations of solids. *Science* 351:aad3000
6. Anisimov VI, Poteryaev AI, Korotin MA, Anokhin AO, Kotliar G. 1997. First-principles calculations of the electronic structure and spectra of strongly correlated systems: dynamical mean-field theory. *Journal of Physics: Condensed Matter* 9:7359
7. Kotliar G, Vollhardt D. 2004. Strongly correlated materials: Insights from dynamical mean-field theory. *Physics Today* 57:53–59
8. Kent PR, Kotliar G. 2018. Toward a predictive theory of correlated materials. *Science* 361:348–354
9. Kotliar G, Savrasov SY, Haule K, Oudovenko VS, Parcollet O, Marianetti CA. 2006. Electronic structure calculations with dynamical mean-field theory. *Rev. Mod. Phys.* 78:865–951
10. Held K. 2007. Electronic structure calculations using dynamical mean field theory. *Advances in physics* 56:829–926

11. Basov DN, Averitt RD, van der Marel D, Dressel M, Haule K. 2011. Electrodynamics of correlated electron materials. *Rev. Mod. Phys.* 83:471–541
12. Georges A, Kotliar G, Krauth W, Rozenberg MJ. 1996. Dynamical mean-field theory of strongly correlated fermion systems and the limit of infinite dimensions. *Rev. Mod. Phys.* 68:13–125
13. Martin R, Reining L, Ceperley D. 2016. Interacting electrons. Cambridge University Press
14. Hohenberg P, Kohn W. 1964. Inhomogeneous electron gas. *Phys. Rev.* 136:B864–B871
15. Ceperley DM, Alder BJ. 1980. Ground state of the electron gas by a stochastic method. *Phys. Rev. Lett.* 45:566–569
16. Perdew JP. 1991. Generalized gradient approximations for exchange and correlation: A look backward and forward. *Physica B: Condensed Matter* 172:1–6
17. Giuliani G, Vignale G, Press CU. 2005. Quantum theory of the electron liquid. Masters Series in Physics and Astronomy. Cambridge University Press
18. Vollhardt D. 2012. Dynamical mean-field theory for correlated electrons. *Annalen der Physik* 524:1–19
19. Anderson PW. 2013. Twenty-five years of high-temperature superconductivity—a personal review. In *Journal of Physics: Conference Series*, vol. 449. IOP Publishing
20. Dagotto E. 2013. Nanoscale phase separation and colossal magnetoresistance: The physics of manganites and related compounds. Springer Series in Solid-State Sciences. Springer Berlin Heidelberg
21. Imada M, Fujimori A, Tokura Y. 1998. Metal-insulator transitions. *Rev. Mod. Phys.* 70:1039–1263
22. Mott NF. 1949. The basis of the electron theory of metals, with special reference to the transition metals. *Proceedings of the Physical Society. Section A* 62:416
23. Terakura K, Oguchi T, Williams AR, Kübler J. 1984. Band theory of insulating transition-metal monoxides: Band-structure calculations. *Phys. Rev. B* 30:4734–4747
24. Gutzwiller MC. 1963. Effect of correlation on the ferromagnetism of transition metals. *Phys. Rev. Lett.* 10:159–162
25. Hubbard J. 1963. Electron correlations in narrow energy bands. *Proc. R. Soc. Lond. A* 276:238–257
26. Kanamori J. 1963. Electron correlation and ferromagnetism of transition metals. *Progress of Theoretical Physics* 30:275–289
27. Lieb EH, Wu FY. 1968. Absence of mott transition in an exact solution of the short-range, one-band model in one dimension. *Phys. Rev. Lett.* 20:1445–1448
28. Pavarini E, Koch E, Vollhardt D, Lichtenstein A. 2014. Dmft at 25: Infinite dimensions: Lecture notes of the autumn school on correlated electrons 2014. Schriften des Forschungszentrums Jülich Reihe Modeling and Simulation. Forschungszentrum Jülich
29. Metzner W, Vollhardt D. 1989. Correlated lattice fermions in $d = \infty$ dimensions. *Phys. Rev. Lett.* 62:324–327
30. Müller-Hartmann E. 1989. The hubbard model at high dimensions: some exact results and weak coupling theory. *Zeitschrift für Physik B Condensed Matter* 76:211–217
31. Georges A, Kotliar G. 1992. Hubbard model in infinite dimensions. *Phys. Rev. B* 45:6479–6483
32. Georges A. 2004. Strongly correlated electron materials: Dynamical mean field theory and electronic structure. *AIP Conference Proceedings* 715:3–74
33. Vollhardt D. 2010. Dynamical mean field theory of electronic correlations in models and materials. *AIP Conference Proceedings* 1297:339–403
34. Jarrell M. 1992. Hubbard model in infinite dimensions: A quantum monte carlo study. *Phys. Rev. Lett.* 69:168–171
35. Anderson PW. 1961. Localized magnetic states in metals. *Phys. Rev.* 124:41–53
36. Haule K. 2018. Structural predictions for correlated electron materials using the functional dynamical mean field theory approach. *Journal of the Physical Society of Japan* 87:041005

37. Marzari N, Mostofi AA, Yates JR, Souza I, Vanderbilt D. 2012. Maximally localized wannier functions: Theory and applications. *Rev. Mod. Phys.* 84:1419–1475
38. Park H, Millis AJ, Marianetti CA. 2014a. Computing total energies in complex materials using charge self-consistent dft + dmft. *Phys. Rev. B* 90:235103
39. Haule K, Yee CH, Kim K. 2010. Dynamical mean-field theory within the full-potential methods: Electronic structure of ceirin 5, cecoin 5, and cerhin 5. *Physical Review B* 81:195107
40. Adler R, Kang CJ, Yee CH, Kotliar G. 2018. Correlated materials design: Prospects and challenges. *Reports on Progress in Physics*
41. Anisimov VI, Zaanen J, Andersen OK. 1991. Band theory and mott insulators: Hubbard U instead of stoner I . *Phys. Rev. B* 44:943–954
42. Karolak M, Ulm G, Wehling T, Mazurenko V, Poteryaev A, Lichtenstein A. 2010. Double counting in LDA+DMFT the example of NiO. *Journal of Electron Spectroscopy and Related Phenomena* 181:11 – 15
43. Dang HT, Ai X, Millis AJ, Marianetti CA. 2014. Density functional plus dynamical mean-field theory of the metal-insulator transition in early transition-metal oxides. *Phys. Rev. B* 90:125114
44. Czyżyk MT, Sawatzky GA. 1994. Local-density functional and on-site correlations: The electronic structure of La_2CuO_4 and $LaCuO_3$. *Phys. Rev. B* 49:14211–14228
45. Park H, Millis AJ, Marianetti CA. 2014b. Total energy calculations using dft+dmft: Computing the pressure phase diagram of the rare earth nickelates. *Phys. Rev. B* 89:245133
46. Haule K. 2015. Exact double counting in combining the dynamical mean field theory and the density functional theory. *Phys. Rev. Lett.* 115:196403
47. Kristanovski O, Shick AB, Lechermann F, Lichtenstein AI. 2018. Role of nonspherical double counting in dft+dmft: Total energy and structural optimization of pnictide superconductors. *Phys. Rev. B* 97:201116
48. Werner P, Comanac A, de’ Medici L, Troyer M, Millis AJ. 2006. Continuous-time solver for quantum impurity models. *Phys. Rev. Lett.* 97:076405
49. Haule K. 2007. Quantum monte carlo impurity solver for cluster dynamical mean-field theory and electronic structure calculations with adjustable cluster base. *Phys. Rev. B* 75:155113
50. Gull E, Millis AJ, Lichtenstein AI, Rubtsov AN, Troyer M, Werner P. 2011. Continuous-time monte carlo methods for quantum impurity models. *Rev. Mod. Phys.* 83:349–404
51. Sémon P, Yee CH, Haule K, Tremblay AMS. 2014. Lazy skip-lists: An algorithm for fast hybridization-expansion quantum monte carlo. *Phys. Rev. B* 90:075149
52. Takizawa M, Minohara M, Kumigashira H, Toyota D, Oshima M, et al. 2009. Coherent and incoherent d band dispersions in srvo 3. *Physical Review B* 80:235104
53. Haule K, Birol T. 2015. Free energy from stationary implementation of the dft+ dmft functional. *Physical review letters* 115:256402
54. Dougier P, Fan JC, Goodenough JB. 1975. Etude des proprietes magnetiques, electriques et optiques des phases de structure perovskite srvo2. 90 et srvo3. *Journal of Solid State Chemistry* 14:247–259
55. Nekrasov I, Held K, Keller G, Kondakov D, Pruschke T, et al. 2006. Momentum-resolved spectral functions of srvo 3 calculated by lda+ dmft. *Physical Review B* 73:155112
56. Hewson AC. 1997. The kondo problem to heavy fermions, vol. 2. Cambridge university press
57. Fazekas P. 1999. Lecture notes on electron correlation and magnetism, vol. 5. World scientific
58. Uehara A, Shinaoka H, Motome Y. 2015. Charge-spin-orbital fluctuations in mixed valence spinels: Comparative study of alv_2o_4 and liv_2o_4 . *Phys. Rev. B* 92:195150
59. Kondo S, Johnston D, Swenson C, Borsa F, Mahajan A, et al. 1997. Liv 2 o 4: A heavy fermion transition metal oxide. *Physical review letters* 78:3729
60. Arita R, Held K, Lukoyanov AV, Anisimov VI. 2007. Doped mott insulator as the origin of heavy-fermion behavior in liv_2o_4 . *Phys. Rev. Lett.* 98:166402
61. Shim J, Haule K, Kotliar G. 2007. Modeling the localized-to-itinerant electronic transition in

- the heavy fermion system CeIrIn₅. *Science* 318:1615–1617
62. Choi HC, Min B, Shim J, Haule K, Kotliar G. 2012. Temperature-dependent Fermi surface evolution in heavy fermion CeIrIn₅. *Physical Review Letters* 108:016402
 63. Kohn W, Sham LJ. 1965. Self-consistent equations including exchange and correlation effects. *Phys. Rev.* 140:A1133–A1138
 64. Baroni S, de Gironcoli S, Dal Corso A, Giannozzi P. 2001. Phonons and related crystal properties from density-functional perturbation theory. *Rev. Mod. Phys.* 73:515–562
 65. Perdew JP, Yue W. 1986. Accurate and simple density functional for the electronic exchange energy: Generalized gradient approximation. *Phys. Rev. B* 33:8800–8802
 66. Perdew JP, Burke K, Ernzerhof M. 1996. Generalized gradient approximation made simple. *Phys. Rev. Lett.* 77:3865–3868
 67. Perdew JP, Ruzsinszky A, Csonka GI, Vydrov OA, Scuseria GE, et al. 2008. Restoring the density-gradient expansion for exchange in solids and surfaces. *Phys. Rev. Lett.* 100:136406
 68. Haas P, Tran F, Blaha P. 2009. Calculation of the lattice constant of solids with semilocal functionals. *Phys. Rev. B* 79:085104
 69. Rabe KM, Ghosez P. 2007. First-principles studies of ferroelectric oxides. In *Physics of ferroelectrics*. Springer, 117–174
 70. Vanderbilt D, Zhong W. 1998. First-principles theory of structural phase transitions for perovskites: competing instabilities. *Ferroelectrics* 206:181–204
 71. Khomskii D. 2014. Transition metal compounds. Cambridge University Press
 72. Dudarev SL, Botton GA, Savrasov SY, Humphreys CJ, Sutton AP. 1998. Electron-energy-loss spectra and the structural stability of nickel oxide: an LSDa+u study. *Phys. Rev. B* 57:1505–1509
 73. Liechtenstein AI, Anisimov VI, Zaanen J. 1995. Density-functional theory and strong interactions: Orbital ordering in Mott-Hubbard insulators. *Phys. Rev. B* 52:R5467–R5470
 74. Rotter M, Tegel M, Johrendt D, Schellenberg I, Hermes W, Pöttgen R. 2008. Spin-density-wave anomaly at 140 K in the ternary iron arsenide BaFe₂As₂. *Phys. Rev. B* 78:020503
 75. Savrasov SY, Kotliar G. 2003. Linear response calculations of lattice dynamics in strongly correlated systems. *Phys. Rev. Lett.* 90:056401
 76. Dai X, Savrasov SY, Kotliar G, Migliori A, Ledbetter H, Abrahams E. 2003. Calculated phonon spectra of plutonium at high temperatures. *Science* 300:953–955
 77. Yin Q, Savrasov SY. 2008. Origin of low thermal conductivity in nuclear fuels. *Phys. Rev. Lett.* 100:225504
 78. Katsnelson MI, Lichtenstein AI. 2000. First-principles calculations of magnetic interactions in correlated systems. *Phys. Rev. B* 61:8906–8912
 79. Lichtenstein A, Katsnelson M, Kotliar G. 2001. Finite-temperature magnetism of transition metals: An ab initio dynamical mean-field theory. *Physical Review Letters* 87:067205
 80. Yang I, Savrasov SY, Kotliar G. 2001. Importance of correlation effects on magnetic anisotropy in Fe and Ni. *Phys. Rev. Lett.* 87:216405
 81. Hirsch JE, Fye RM. 1986. Monte Carlo method for magnetic impurities in metals. *Physical Review Letters* 56:2521
 82. Leonov I, Poteryaev AI, Anisimov VI, Vollhardt D. 2011. Electronic correlations at the α - γ structural phase transition in paramagnetic iron. *Phys. Rev. Lett.* 106:106405
 83. Leonov I, Poteryaev AI, Anisimov VI, Vollhardt D. 2012. Calculated phonon spectra of paramagnetic iron at the α - γ phase transition. *Phys. Rev. B* 85:020401
 84. Leonov I, Poteryaev A, Gornostyrev YN, Lichtenstein A, Katsnelson M, et al. 2014. Electronic correlations determine the phase stability of iron up to the melting temperature. *Scientific reports* 4:5585
 85. Han Q, Birol T, Haule K. 2018. Phonon softening due to melting of the ferromagnetic order in elemental iron. *Phys. Rev. Lett.* 120:187203
 86. Haule K, Pascut GL. 2016. Forces for structural optimizations in correlated materials within

- a dft+embedded dmft functional approach. *Phys. Rev. B* 94:195146
87. Thornton G, Tofield B, Hewat A. 1986. A neutron diffraction study of LaCoO_3 in the temperature range 4.2 K to 1248 K. *Journal of Solid State Chemistry* 61:301–307
 88. Chakrabarti B, Birol T, Haule K. 2017. Role of entropy and structural parameters in the spin-state transition of LaCoO_3 . *Phys. Rev. Materials* 1:064403
 89. Satija SK, Comès RP, Shirane G. 1985. Neutron scattering measurements of phonons in iron above and below T_c . *Phys. Rev. B* 32:3309–3311
 90. Bain EC, Dunkirk N. 1924. The nature of martensite. *trans. AIME* 70:25–47
 91. Neuhaus J, Petry W, Krimmel A. 1997. Phonon softening and martensitic transformation in α -Fe. *Physica B: Condensed Matter* 234:897–899
 92. Zunger A, Wei SH, Ferreira LG, Bernard JE. 1990. Special quasirandom structures. *Phys. Rev. Lett.* 65:353–356
 93. Trimarchi G, Wang Z, Zunger A. 2018. Polymorphous band structure model of gapping in the antiferromagnetic and paramagnetic phases of the Mott insulators MnO , FeO , CoO , and NiO . *Phys. Rev. B* 97:035107
 94. Körmann F, Dick A, Grabowski B, Hickel T, Neugebauer J. 2012. Atomic forces at finite magnetic temperatures: Phonons in paramagnetic iron. *Phys. Rev. B* 85:125104
 95. Ikeda Y, Seko A, Togo A, Tanaka I. 2014. Phonon softening in paramagnetic bcc Fe and its relationship to the pressure-induced phase transition. *Phys. Rev. B* 90:134106
 96. Körmann F, Grabowski B, Dutta B, Hickel T, Mauger L, et al. 2014. Temperature dependent magnon-phonon coupling in bcc Fe from theory and experiment. *Phys. Rev. Lett.* 113:165503
 97. Luo W, Johansson B, Eriksson O, Arapan S, Souvatzis P, et al. 2010. Dynamical stability of body center cubic iron at the earth's core conditions. *Proceedings of the National Academy of Sciences*
 98. Lian CS, Wang JT, Chen C. 2015. Ab initio study of the anharmonic lattice dynamics of iron at the $\gamma - \delta$ phase transition. *Phys. Rev. B* 92:184110
 99. Kuneš J, Lukoyanov AV, Anisimov VI, Scalettar RT, Pickett WE. 2008. Collapse of magnetic moment drives the Mott transition in MnO . *Nature materials* 7:198
 100. Leonov I, Binggeli N, Korotin D, Anisimov VI, Stojić N, Vollhardt D. 2008. Structural relaxation due to electronic correlations in the paramagnetic insulator KCuF_3 . *Phys. Rev. Lett.* 101:096405
 101. Park H, Millis AJ, Marianetti CA. 2012. Site-selective Mott transition in rare-earth-element nickelates. *Physical review letters* 109:156402
 102. Haule K, Pascut GL. 2017. Mott transition and magnetism in rare earth nickelates and its fingerprint on the x-ray scattering. *Scientific reports* 7:10375
 103. Bärnighausen H, Schiller G. 1985. The crystal structure of $\text{a-Fe}_2\text{O}_3$. *Journal of the Less Common Metals* 110:385–390
 104. Heyd J, Scuseria GE. 2004. Assessment and validation of a screened Coulomb hybrid density functional. *The Journal of chemical physics* 120:7274–7280
 105. Adamo C, Barone V. 1999. Toward reliable density functional methods without adjustable parameters: The PBE0 model. *The Journal of chemical physics* 110:6158–6170
 106. Perdew JP, Ernzerhof M, Burke K. 1996. Rationale for mixing exact exchange with density functional approximations. *The Journal of chemical physics* 105:9982–9985
 107. Heyd J, Scuseria GE, Ernzerhof M. 2003. Hybrid functionals based on a screened Coulomb potential. *The Journal of chemical physics* 118:8207–8215
 108. Becke AD. 1993. Density-functional thermochemistry. iii. the role of exact exchange. *The Journal of chemical physics* 98:5648–5652
 109. Paier J, Marsman M, Kresse G. 2007. Why does the B3LYP hybrid functional fail for metals? *The Journal of chemical physics* 127:024103
 110. Paier J, Marsman M, Hummer K, Kresse G, Gerber IC, Ángyán JG. 2006. Screened hybrid density functionals applied to solids. *The Journal of chemical physics* 124:154709

111. Da Silva JLF, Ganduglia-Pirovano MV, Sauer J, Bayer V, Kresse G. 2007. Hybrid functionals applied to rare-earth oxides: The example of ceria. *Phys. Rev. B* 75:045121
112. Jacob D, Haule K, Kotliar G. 2008. Combining the hybrid functional method with dynamical mean-field theory. *EPL (Europhysics Letters)* 84:57009
113. Onida G, Reining L, Rubio A. 2002. Electronic excitations: density-functional versus many-body green's-function approaches. *Rev. Mod. Phys.* 74:601–659
114. Kotliar G, Savrasov S. 2001. Model hamiltonians and first principles electronic structure calculations. In *New Theoretical Approaches to Strongly Correlated Systems*. Springer, 259–301
115. Biermann S, Aryasetiawan F, Georges A. 2003. First-principles approach to the electronic structure of strongly correlated systems: Combining the *gw* approximation and dynamical mean-field theory. *Phys. Rev. Lett.* 90:086402
116. Tomczak JM, Casula M, Miyake T, Aryasetiawan F, Biermann S. 2012. Combined *gw* and dynamical mean-field theory: Dynamical screening effects in transition metal oxides. *EPL (Europhysics Letters)* 100:67001
117. Tomczak JM, Casula M, Miyake T, Biermann S. 2014. Asymmetry in band widening and quasiparticle lifetimes in srvo3: Competition between screened exchange and local correlations from combined *g w* and dynamical mean-field theory *g w*+ dmft. *Physical Review B* 90:165138
118. Taranto C, Kaltak M, Parragh N, Sangiovanni G, Kresse G, et al. 2013. Comparing quasiparticle *gw*+dmft and lda+dmft for the test bed material srvo₃. *Phys. Rev. B* 88:165119
119. Hansmann P, Ayrat T, Vaugier L, Werner P, Biermann S. 2013. Long-range coulomb interactions in surface systems: A first-principles description within self-consistently combined *gw* and dynamical mean-field theory. *Phys. Rev. Lett.* 110:166401
120. Choi S, Kutepov A, Haule K, van Schilfhaarde M, Kotliar G. 2016. First-principles treatment of mott insulators: linearized qsgw+ dmft approach. *Npj Quantum Materials* 1:16001
121. Sémon P, Haule K, Kotliar G. 2017. Validity of the local approximation in iron pnictides and chalcogenides. *Phys. Rev. B* 95:195115
122. Goodenough JB. 1971. The two components of the crystallographic transition in vo₂. *Journal of Solid State Chemistry* 3:490–500
123. Eyert V. 2002. The metal-insulator transitions of vo₂: A band theoretical approach. *Annalen der Physik* 11:650–704
124. Weber C, O'Regan DD, Hine NDM, Payne MC, Kotliar G, Littlewood PB. 2012. Vanadium dioxide: A peierls-mott insulator stable against disorder. *Phys. Rev. Lett.* 108:256402
125. Biermann S, Poteryaev A, Lichtenstein AI, Georges A. 2005. Dynamical singlets and correlation-assisted peierls transition in vo₂. *Phys. Rev. Lett.* 94:026404
126. Lazarovits B, Kim K, Haule K, Kotliar G. 2010. Effects of strain on the electronic structure of vo 2. *Physical Review B* 81:115117
127. Brito W, Aguiar M, Haule K, Kotliar G. 2016. Metal-insulator transition in vo 2: a dft+ dmft perspective. *Physical review letters* 117:056402
128. Brito W, Aguiar M, Haule K, Kotliar G. 2017. Dynamic electronic correlation effects in nbo 2 as compared to vo 2. *Physical Review B* 96:195102
129. Franceschetti A, Zunger A. 1999. The inverse band-structure problem of finding an atomic configuration with given electronic properties. *Nature* 402:60